PHYSICAL REVIEW B **93**, 100201(R) (2016)

Shape dependence of transmission, reflection, and absorption eigenvalue densities in disordered waveguides with dissipation

A. Yamilov,[1,*] S. Petrenko,[1] R. Sarma,[2] and H. Cao[2,†]

[1]*Department of Physics, Missouri University of Science and Technology, Rolla, Missouri 65409, USA*

[2]*Department of Applied Physics, Yale University, New Haven, Connecticut 06520, USA*

(Received 3 November 2015; revised manuscript received 12 February 2016; published 3 March 2016)

The universal bimodal distribution of transmission eigenvalues in lossless diffusive systems underpins such celebrated phenomena as universal conductance fluctuations, quantum shot noise in condensed matter physics, and enhanced transmission in optics and acoustics. Here, we show that in the presence of absorption, the density of the transmission eigenvalues depends on the confinement geometry of the scattering media. Furthermore, in an asymmetric waveguide, the densities of the reflection and absorption eigenvalues also depend on the side from which the waves are incident. With increasing absorption, the density of absorption eigenvalues transforms from a single-peak to a double-peak function. Our findings open an additional avenue for coherent control of wave transmission, reflection, and absorption in random media.

DOI: 10.1103/PhysRevB.93.100201

Mesoscopic electronic transport through a disordered conductor can be described by a $N \times N$ transmission matrix $\hat{t}$ which relates the amplitudes of N incoming and outgoing transverse modes [1]. The dimensionless conductance is $g = \langle \mathrm{Tr}(\hat{t}^\dagger \hat{t}) \rangle = \sum_n \langle \tau_n \rangle$, where τ_n are the eigenvalues of the matrix $\hat{t}^\dagger \hat{t}$ [2] and $\langle \cdots \rangle$ denotes the ensemble average. Therefore, electron transport in a metallic wire can be viewed as a parallel transmission over N orthogonal eigenchannels with individual transmissions of τ_n. Due to the mesoscopic correlations [3,4], the density of the transmission eigenvalues $\mathcal{D}(\tau)$ has a bimodal functional form [5–11] with peaks at $\tau \to 0$ and $\tau \to 1$ [12,13]. This leads to, e.g., universal conductance fluctuations [14,15] and quantum shot noise [16,17]. In Ref. [18], bimodal distribution was proven to be applicable to an arbitrary geometry of the conductor as long as the transport remains diffusive and free of dissipation.

The bimodal distribution obtained in the context of mesoscopic physics is also applicable to the transport of classical waves in scattering media [19]. In optics, the rapid development of wave-front shaping techniques has enabled experimental access to transmission eigenchannels [20] that allows control of the total transmission [21–23] as well as focusing through turbid media [24–31]. Absorption, common in optics, breaks energy conservation and makes the density of transmission eigenvalues [32] as well as reflection [33–35] eigenvalues to depend on its strength. However, the questions of whether the geometry of the system could affect the eigenvalue density in dissipative systems and, if so, how it would affect it, still need to be addressed.

In this Rapid Communication we demonstrate that, unlike passive systems, the density of the transmission eigenvalues in absorbing disordered waveguides is geometry dependent, that is beyond predictions of the existing theory [32]. This opens the possibility of tuning the functional form of the eigenvalue density by choosing the shape of the boundary. Furthermore, we show that dissipation makes a profound impact on the densities of reflection eigenvalues ρ and absorption eigenvalues α that can even depend on which side of the waveguide is being illuminated in the case of an asymmetric waveguide shape. This is attributed to the fact that reflection matrices for illumination from different sides are no longer related in the presence of dissipation. Above a certain absorption threshold, the density of absorption eigenvalues exhibits a qualitative transformation from a single-peak to a double-peak function. The additional peak at $\alpha \simeq 1$ enables a nearly complete absorption at any frequency with an appropriate input wave front.

Transmission eigenvalues. We consider a variable width waveguide, schematically depicted in the inset of Fig. 1(a), formed by reflecting boundaries at $y(z) = \pm W(z)/2$, where $W(z)$ is a smooth function of z. The leads on the left/right support N_L/N_R propagating modes. The transport through the disordered region $0 \leqslant z \leqslant L$ is described by a complex $N_R \times N_L$ matrix $\hat{t}$. For passive random media, the density of the eigenvalues of matrix $\hat{t}^\dagger \hat{t}$ is $\mathcal{D}(\tau) = (g_p/2)\tau^{-1}(1-\tau)^{-1/2}$. In Ref. [36], we reproduce this result using the circuit theory of Ref. [18] with the dimensionless conductance given by $g_p[W(z)] = (k\ell/2)[\int_0^L W^{-1}(z)dz]^{-1}$, where $k = 2\pi/\lambda$ is the wave number, ℓ is the transport mean free path, and subscript p stands for "passive." For a waveguide with constant $W = N(\lambda/2)$ width we recover the well-known expression $g_p = (\pi/2)N\ell/L$ [37].

Figure 1(a) schematically depicts $\mathcal{D}(\tau)$ with three contributions from open, closed, and evanescent eigenchannels. Open channels correspond to eigenvalues close to unity ($\tau_O < \tau < 1$) and closed channels correspond to low transmission ($\tau_C < \tau < \tau_O$). Defining $\int_{\tau_O}^1 P(\tau)d\tau = g_p$ [12] gives $\tau_O \equiv [2e/(e^2+1)]^2 \simeq 0.42$. Together, open and closed channels are described by the bimodal distribution. The cutoff τ_C at the level of ballistic transmission [5,37] is obtained by normalizing $\int_{\tau_C}^1 \mathcal{D}(\tau)d\tau$ to the number of propagating channels $N_{\min} = W_{\min}/(\lambda/2)$ [see Fig. 1(a)]. In a waveguide with a constriction, there are $\min(N_L, N_R)$ transmission eigenchannels, among which $N_E = \min(N_L, N_R) - N_{\min}$ are evanescent channels with intensity decaying on the scale of the wavelength inside the narrow portion of the waveguide and, therefore, $\tau \ll \tau_C$

*yamilov@mst.edu

†hui.cao@yale.edu

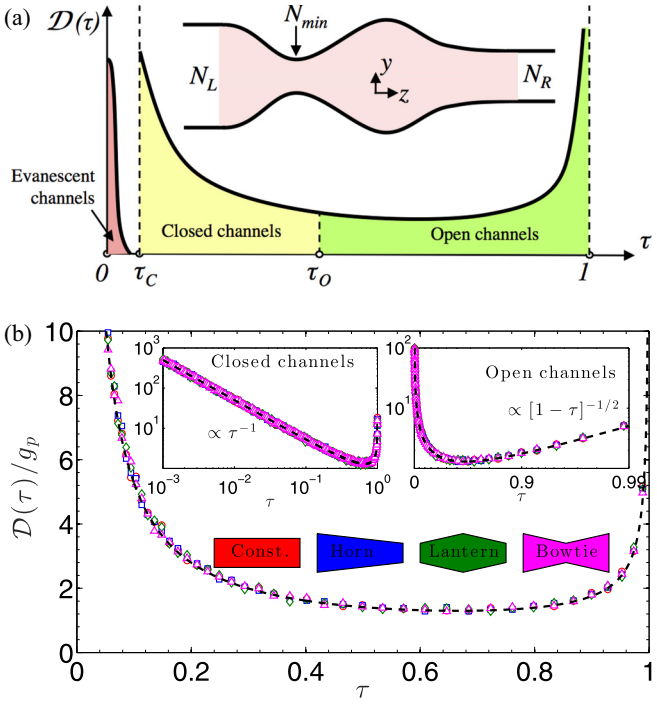

FIG. 1. (a) Schematic illustration of density of the transmission eigenvalues $\mathcal{D}(\tau)$ in a passive disordered waveguide of varying width $W(z)$ drawn in the inset. It is made up of open ($\tau_O < \tau \leqslant 1$), closed ($\tau_C < \tau < \tau_O$), and evanescent ($\tau < \tau_C$) eigenchannels. (b) Normalized density of the transmission eigenvalues $\mathcal{D}(\tau)/g_p$ computed numerically for the four passive waveguides shown. All data points fall onto the dashed line—the bimodal distribution. The two insets show that the bimodal distribution correctly describes both $\tau \to 0$ (closed channels) and $\tau \to 1$ (open channels) limits, regardless of the waveguide shape.

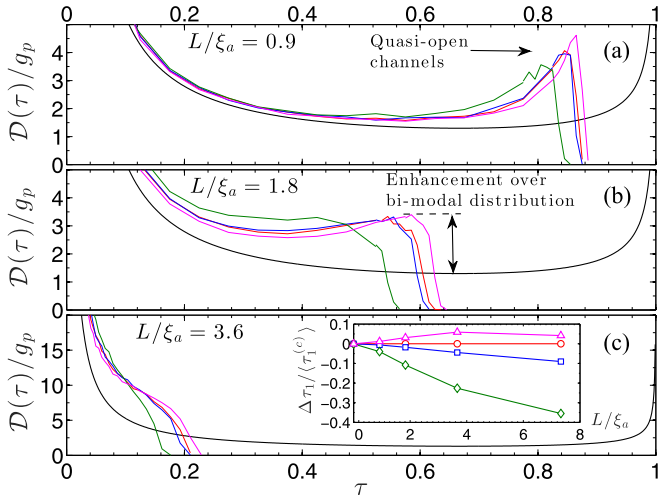

FIG. 2. Density of the transmission eigenvalues $\mathcal{D}(\tau)/g_p$ in absorbing diffusive waveguides depends not only on the absorption strength but also on the confinement geometry. The four colored curves correspond to four waveguides with matched color in Fig. 1(b). The absorption strength is $L/\xi_a = 0.9$ (a), 1.8 (b), and 3.6 (c). The universal bimodal distribution of passive waveguides (solid line) is shown for reference. Inset of (c): Normalized deviation of maximum transmission eigenvalue $\Delta\tau_1 = \langle\tau_1\rangle - \langle\tau_1^{(c)}\rangle$ in four waveguides of different shapes from that in the rectangular waveguide $\langle\tau_1^{(c)}\rangle$, as a function of absorption L/ξ_a.

for these channels [36]. This boundary separating evanescent and closed channels is exaggerated for illustration in Fig. 1(a), as in practice $\tau_C \simeq 0$.

The applicability of the bimodal distribution for open and closed channels is confirmed in Fig. 1(b). It shows $\mathcal{D}(\tau)/g_p$ computed numerically using the KWANT simulation package [38] (see Ref. [36] for details) for four waveguides of different shapes (drawn in the inset): a rectangular waveguide of width $W = 273 \times (\lambda/2)$; a horn waveguide of width linearly decreasing from $W_L = 400 \times (\lambda/2)$ to $W_R = 200 \times (\lambda/2)$; a lantern waveguide of width linearly tapered from $W_M = 400 \times (\lambda/2)$ in the middle to $W_L = W_R = 200 \times (\lambda/2)$ at the two ends; and a bowtie of width tapered from $W_L = W_R = 400 \times (\lambda/2)$ at the ends to $W_M = 200 \times (\lambda/2)$ in the middle. The conductance in the four systems is $g_p = 13.9$, 14.2, 13.5, and 13.9, respectively. The other system parameters are $L/\ell \simeq 31$, $k\ell \simeq 60$, $L/\lambda \simeq 300$. We accumulate ensembles of $\sim 5 \times 10^5$ eigenvalues so that their densities are free of noise over at least five decades of magnitude.

Figure 1(b) clearly shows that the bimodal distribution, including the asymptotes for $\tau \to 0, 1$ in the insets of Fig. 1(b), describes open and closed eigenchannels in waveguides of different shapes without any fitting parameters. The nonuniversal contribution of evanescent channels to $\mathcal{D}(\tau \simeq 0)$ cannot be clearly distinguished from the peak of closed channels in the numerical data because $\tau_C \sim \exp(-L/\ell) \sim \exp(-31)$ cannot be resolved. Nevertheless, the evanescent channels can make up a substantial fraction of the total channels, e.g., in the bowtie waveguide, one half of the transmission eigenchannels are evanescent and have the vanishingly small values of τ.

Absorption breaks flux conservation and time-reversal symmetry, leaving optical reciprocity the only constraint on the scattering matrix $\hat{S}$ of the system [39]. In Ref. [36] we show that it relates (in each realization of disorder) the transmission matrices for waves incident from the left $\hat{t}$ and right $\hat{t}'$ as $\hat{t}^T = \hat{t}'$, where superscript T denotes the matrix transpose. This relationship signifies that even in the presence of absorption, $\hat{t}^\dagger\hat{t}$ and $\hat{t}'^\dagger\hat{t}'$ have the same set of nonzero eigenvalues.

Figures 2(a)–2(c) show the density of the transmission eigenvalues for waveguides of different shapes with three values of absorption: $L/\xi_a = 0.9, 1.8$, and 3.6. $\xi_a = [\ell\ell_a/2]^{1/2}$ is the diffusive absorption length and ℓ_a is the ballistic absorption length. Common to all geometries, $\tau \simeq 1$ eigenvalues are attenuated so that the density no longer reaches unity. Instead, the maximum eigenvalue $\langle\tau_1\rangle < 1$. Open channels are redistributed throughout the $\tau_C < \tau < \max(\tau_1)$ interval so that the eigenvalue density is consistently higher than that in passive systems. However, unlike the bimodal distribution for the passive systems [see Fig. 1(b)], $\mathcal{D}(\tau)$ *is no longer universal and exhibits a clear shape dependence*. The maximum transmission eigenvalue is lowest for the lantern geometry. Such behavior can be understood as the narrower openings and slanted walls of the lantern waveguide reduce the escape probability and increase the effective absorption, leading to smaller $\langle\tau_1\rangle$. In contrast, the situation is reversed in the bowtie waveguide (see Fig. 2). This structure has

wider openings and, therefore, waves are more likely to escape without being strongly attenuated. The normalized deviation of the largest eigenvalue $\langle\tau_1\rangle$ in waveguides of different shapes from that in the rectangular waveguide $\langle\tau_1^{(c)}\rangle$ is plotted in the inset of Fig. 2(c). The deviation increases with absorption strength and can be either negative (horn, lantern) or positive (bowtie). However, at the largest value of absorption of $L/\xi_a \simeq 7.3$, the deviation is reduced in the bowtie waveguide, which can be understood as follows. For strong absorption $L \gg \xi_a$, short propagation paths dominate transport [29], so we expect the deviation to decrease in this limit because all geometries have the same length L. Such ballisticlike propagation is more favored due to the constriction in the bowtie waveguide, where this transition occurs first.

Reflection eigenvalues. In a passive system, the energy conservation and symmetry requirements make all nonzero eigenvalues of $\hat{t}^\dagger\hat{t}$, $\hat{I}-\hat{r}^\dagger\hat{r}$, $\hat{t}'^\dagger\hat{t}'$, $\hat{I}-\hat{r}'^\dagger\hat{r}'$ identical, where $\hat{r}$ ($\hat{r}'$) represents the reflection matrix for waves incident from the left (right) end of the waveguide [36]. This leads to the bimodal distribution of the density of $1-\rho$ for both left and right reflection eigenvalues ρ and regardless of the shape of the waveguide. In an asymmetric waveguide with $N_L \neq N_R$ (we will assume $N_L > N_R$ without loss of generality), the $N_L \times N_L$ matrix $\hat{r}^\dagger\hat{r}$ also has $N_L - N_R$ eigenvalues with $\rho = 1$, giving the *perfectly reflecting eigenchannels* for light incident from the left (wider opening). Meanwhile, for waves incident from the right (narrower opening), there are no perfectly reflecting eigenchannels because the $N_R \times N_R$ matrix $\hat{r}'^\dagger\hat{r}'$ has only N_R eigenvalues, all of which have corresponding transmission eigenvalues that are nonzero. The results of the numerical simulations in passive waveguides of different shapes (cf. Fig. 3) confirm that the density of both left/right reflection eigenvalues $\mathcal{D}(1-\rho)$ follows the universal bimodal distribution, which still holds in asymmetric waveguides as the perfectly reflecting eigenchannels only have a singular contribution at $\rho = 1$.

Due to the absence of flux conservation in systems with absorption, the links between reflection and transmission matrices *and* between left/right reflection matrices are severed [36]. Consequently, in each disorder realization, the eigenvalues of $\hat{r}^\dagger\hat{r}$ and $\hat{r}'^\dagger\hat{r}'$ are not necessarily identical and they are no longer related to the transmission eigenvalues. Our numerical simulations confirm that the perfect reflecting channels are removed by absorption as *all* reflection eigenvalues become less than unity. Furthermore, in asymmetric waveguides ($N_L \neq N_R$), the densities of reflection eigenvalues differ for waves incident from the left/right side of the waveguide, as shown in Figs. 3(a) and 3(b) for the horn geometry. Even for symmetric waveguides ($N_L = N_R$), $\mathcal{D}(\rho)$ is still clearly shape dependent, as seen in Figs. 3(a) and 3(b) for the rectangular, lantern, and bowtie geometries: $\mathcal{D}(1-\rho)$ are distinctly different in the $(1-\rho)\to 0$ limit while in the limit $(1-\rho)\to 1$ the difference is greatly reduced. The attenuation of reflection by absorption depends on how strong the light is coupled into the absorbing waveguide, which can be controlled by the waveguide geometry. For example, the narrower opening and slanted sidewall of a lantern waveguide reduces the coupling of incident light, as compared to the bowtie waveguide.

Figure 3(b) shows that power exponent in $\mathcal{D}(1-\rho)\propto\rho^{-1}$ for $(1-\rho)\to 1$ is independent of the waveguide shape/input direction and it is the same as in a passive system. For $(1-\rho)\to(1-\rho_{\max})$, we find that the power exponent in $\mathcal{D}(1-\rho)\propto(1-\rho)^{-1.35}$ has a weak shape dependence. The value 1.35 is smaller than 3/2 found in Refs. [33,34] for $a = N\ell/\ell_a \gg 1$ in rectangular waveguides. We attribute the discrepancy to an insufficiently large value of $a = 1.9$ for the case shown in Fig. 3(a).

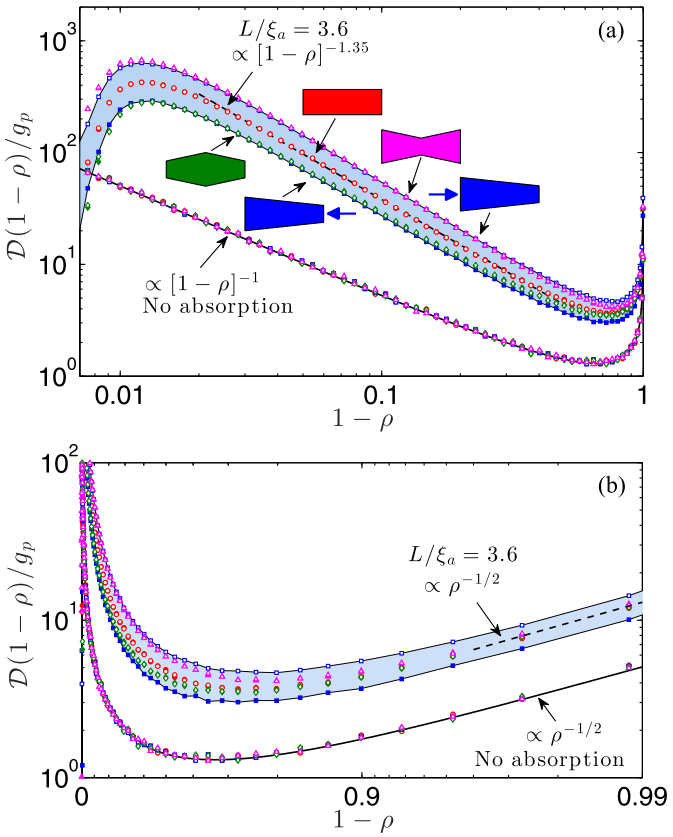

FIG. 3. Density $\mathcal{D}(1-\rho)/g_p$ of the reflection eigenvalues ρ in diffusive waveguides of different shapes with absorption ($L/\xi_a = 3.6$) and without absorption. (a) and (b) show the power scaling behaviors at $(1-\rho)\to 0$ and 1, respectively. Without absorption, all eigenvalue densities, regardless of the waveguide shape or input direction, fall onto the bimodal distribution—solid curve. In absorbing systems, $\mathcal{D}(1-\rho)/g_p$ obtained for waves incident from the left/right are shown with open/solid symbols. For all symmetric waveguides (rectangular, lantern, bowtie) with absorption, $N_L = N_R$, solid and open symbols coincide. For the asymmetric horn waveguide ($N_L \neq N_R$), a large disparity between left/right illumination is highlighted by the shaded area.

Absorption eigenvalues. In a dissipative system, the nonunitary part of the scattering matrix $\hat{I}-\hat{S}^\dagger\hat{S}\equiv\hat{A}_S$ accounts for absorption [40] and its largest eigenvalue $\alpha_{S,1}$ tells the maximum absorption that can be achieved by shaping the input wave front [30]. This requires controlling all modes incident onto both sides of the waveguide. However, more common in experiments is only one side of the system is illuminated. In such a case the matrix $\hat{A}=\hat{I}-\hat{r}^\dagger\hat{r}-\hat{t}^\dagger\hat{t}$ describes the absorption of input light. Its largest eigenvalue α_1 determines the maximum absorption in a given system when only one side is accessible. Similar to the density of the reflection eigenvalues, $\mathcal{D}(\alpha)$ depends on the shape of the waveguide

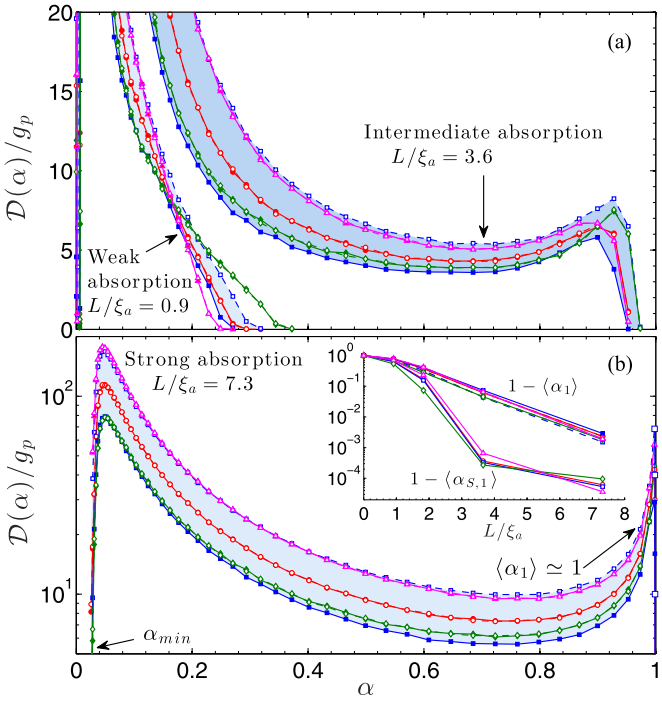

FIG. 4. Density $\mathcal{D}(\alpha)$ of absorption eigenvalues α in disordered waveguides of different shapes, under one-sided illumination, evolves from a one-peak function at weak absorption (the ensemble-averaged maximum absorption eigenvalue $\langle\alpha_1\rangle \ll 1$) to a double-peak function at intermediate absorption ($\langle\alpha_1\rangle \lesssim 1$) in (a), and the second peak moves to $\alpha \simeq 1$ at strong absorption ($\langle\alpha_1\rangle \simeq 1$) in (b). Symbol notations are the same as in Fig. 3. In all cases the normalized density of the absorption eigenvalues exhibits a strong dependence on the shape of the waveguide, and for the asymmetric (horn) waveguide also on the input direction. The inset in (b) plots the ensemble-averaged maximum absorption eigenvalue $\langle\alpha_1\rangle$ vs the absorption strength L/ξ_a. For comparison, the maximum absorption eigenvalues $\langle\alpha_{S,1}\rangle$ for two-sided illumination are also shown.

and the input direction [cf. Figs. 4(a) and 4(b)]. Common to all geometries, the functional form of $\mathcal{D}(\alpha)$ undergoes a qualitative change with an increase of absorption strength. At weak absorption, the eigenvalue density monotonously decreases toward zero with an increase of α [cf. Fig. 4(a)]. At the increased absorption, the density develops the second maximum at $\alpha \simeq 1$. Even in this regime, there exists an upper bound which approaches unity exponentially [cf. the inset of Fig. 4(b)]. A coherent perfect absorber proposed in Ref. [41] achieves 100% absorption but requires full control of the incident wave front and a specific amount of absorption. In contrast, we show that at any frequency and with any absorption (above a certain threshold) the maximum achievable absorption with one-sided excitation α_1 can be close to unity. Moreover, with the left end of the waveguide being illuminated, for example, we can achieve nearly perfect absorption by controlling a fraction $N_L/(N_L + N_R)$ of all input channels, that can be small in, e.g., a horn waveguide with $N_L < N_R$.

We note that the absorption dependence of the maximum eigenvalue $\langle\alpha_1\rangle$ for one-sided illumination is qualitatively different from $\langle\alpha_{S,1}\rangle$ for two-sided illumination [cf. the inset of Fig. 4(b)]. The former approaches unity exponentially, $1 - \langle\alpha_1\rangle \propto \exp[-L/\xi_a]$. In contrast, excitation from both sides results in a sharp transition at $L/\xi_a \sim 3$, above which the strong enhancement of absorption [30] with $\langle\alpha_{S,1}\rangle \simeq 1$ becomes possible. The critical value of the absorption can be estimated by comparing the diffusion time without absorption $L^2/D\pi^2$ to the absorption time $t_a = \xi_a^2/D$, where D is the diffusion coefficient. Equating these two characteristic time scales results in $L/\xi_a = \pi$, which agrees with Fig. 4(b). This offers an absorption analogy with a diffusive random laser [42–44] where exactly the same amount of gain corresponds to the lasing threshold, giving *output* to all sides.

Conclusions. We believe our results will have profound implications for coherent control of wave transmission, reflection, and absorption in random media [20,45]. The ability to modify the eigenvalue densities will greatly enhance the capability of coherent control, with applications to imaging through opaque media and targeted deposition of energy inside turbid media. Furthermore, nanophotonic waveguides with various geometries can be readily made with current nanofabrication techniques [46], and the control of light transmission or reflection by shaping the incident wave front will enable different functionalities for photonic applications.

We thank A. D. Stone, P. Brouwer, and C. W. J. Beenakker for stimulating discussions, and B. van Heck for technical help with the KWANT simulation package. This work is supported by the National Science Foundation under Grants No. DMR-1205307 and No. DMR-1205223.

[1] R. Landauer, Philos. Mag.**21**, 863 (2006).
[2] D. S. Fisher and P. A. Lee, Phys. Rev. B **23**, 6851 (1981).
[3] R. Berkovits and S. Feng, Phys. Rep. **238**, 135 (1994).
[4] M. C. van Rossum and T. M. Nieuwenhuizen, Rev. Mod. Phys. **71**, 313 (1999).
[5] O. N. Dorokhov, Solid State Commun. **51**, 381 (1984).
[6] J. L. Pichard and G. André, Europhys. Lett. **2**, 477 (1986).
[7] K. A. Muttalib, J. L. Pichard, and A. D. Stone, Phys. Rev. Lett. **59**, 2475 (1987).
[8] P. A. Mello and J. L. Pichard, Phys. Rev. B **40**, 5276 (1989).
[9] C. W. J. Beenakker and B. Rajaei, Phys. Rev. B **49**, 7499 (1994).
[10] A. Altland, A. Kamenev, and C. Tian, Phys. Rev. Lett. **95**, 206601 (2005).
[11] B. Gérardin, J. Laurent, A. Derode, C. Prada, and A. Aubry, Phys. Rev. Lett. **113**, 173901 (2014).
[12] Y. Imry, Europhys. Lett. **1**, 249 (1986).
[13] J. B. Pendry, A. MacKinnon, and P. J. Roberts, Proc. R. Soc. London, Ser. A **437**, 67 (1992).
[14] P. A. Lee and A. D. Stone, Phys. Rev. Lett. **55**, 1622 (1985).
[15] *Mesoscopic Phenomena in Solids*, edited by B. L. Altshuler, P. A. Lee, and R. A. Webb (North-Holland, Amsterdam, 1991).

[16] C. W. J. Beenakker and M. Büttiker, Phys. Rev. B **46**, 1889 (1992).
[17] B. L. Altshuler, L. S. Levitov, and A. Y. Yakovets, Pis'ma Zh. Eksp. Teor. Fiz. **59**, 821 (1994) [JETP Lett. **59**, 857 (1994)].
[18] Y. V. Nazarov, Phys. Rev. Lett. **73**, 134 (1994).
[19] E. Akkermans and G. Montambaux, *Mesoscopic Physics of Electrons and Photons* (Cambridge University Press, Cambridge, U.K., 2007).
[20] P. A. Mosk, A. Lagendijk, G. Lerosey, and M. Fink, Nat. Photonics **6**, 283 (2012).
[21] M. Kim, Y. Choi, C. Yoon, W. Choi, J. Kim, Q. H. Park, and W. Choi, Nat. Photonics **6**, 581 (2012).
[22] H. Yu, T. R. Hillman, W. Choi, J. O. Lee, M. S. Feld, R. R. Dasari, and Y. K. Park, Phys. Rev. Lett. **111**, 153902 (2013).
[23] S. M. Popoff, A. Goetschy, S. F. Liew, A. D. Stone, and H. Cao, Phys. Rev. Lett. **112**, 133903 (2014).
[24] I. M. Vellekoop and A. P. Mosk, Phys. Rev. Lett. **101**, 120601 (2008).
[25] Z. Shi and A. Z. Genack, Phys. Rev. Lett. **108**, 043901 (2012).
[26] S. M. Popoff, G. Lerosey, R. Carminati, M. Fink, A. C. Boccara, and S. Gigan, Phys. Rev. Lett. **104**, 100601 (2010).
[27] T. Kohlgraf-Owens and A. Dogariu, Opt. Lett. **35**, 2236 (2010).
[28] O. Katz, E. Small, Y. Bromberg, and Y. Silberberg, Nat. Photonics **5**, 372 (2011).
[29] S. F. Liew, S. M. Popoff, A. P. Mosk, W. L. Vos, and H. Cao, Phys. Rev. B **89**, 224202 (2014).
[30] Y. D. Chong and A. D. Stone, Phys. Rev. Lett. **107**, 163901 (2011).
[31] X. Cheng and A. Z. Genack, Opt. Lett. **39**, 6324 (2014).
[32] P. W. Brouwer, Phys. Rev. B **57**, 10526 (1998).
[33] N. A. Bruce and J. T. Chalker, J. Phys. A **29**, 3761 (1996).
[34] C. W. J. Beenakker, J. C. J. Paasschens, and P. W. Brouwer, Phys. Rev. Lett. **76**, 1368 (1996).
[35] A. Goetschy and A. D. Stone, Phys. Rev. Lett. **111**, 063901 (2013).
[36] See Supplemental Material at http://link.aps.org/supplemental/10.1103/PhysRevB.93.100201 for (i) derivation of the density of transmission eigenvalues in passive waveguides with an arbitrary shape; (ii) discussion of properties of the scattering matrix of dissipative waveguides with varying cross-section; (iii) details of numerical simulations; (iv) demonstration of invariance of density of transmission eigenvalues in rectangular waveguides in the crossover from quasi-1D to 2D geometry; (v) analysis of density of absorption eigenvalues with two-sided excitation; and (vi) review of the existing theoretical description of the density of the transmission eigenvalues in rectangular waveguides with absorption.
[37] C. W. Beenakker, Rev. Mod. Phys. **69**, 731 (1997).
[38] C. W. Groth, M. Wimmer, A. R. Akhmerov, and X. Waintal, New J. Phys. **16**, 063065 (2014).
[39] R. Carminati, J. J. Sáenz, J.-J. Greffet, and M. Nieto-Vesperinas, Phys. Rev. A **62**, 012712 (2000).
[40] C. W. J. Beenakker, Phys. Rev. Lett. **81**, 1829 (1998).
[41] Y. D. Chong, L. Ge, H. Cao, and A. D. Stone, Phys. Rev. Lett. **105**, 053901 (2010).
[42] N. M. Lawandy, R. M. Balachandran, A. S. L. Gomes, and E. Sauvain, Nature (London) **368**, 436 (1994).
[43] H. Cao, in *Progress in Optics*, edited by E. Wolf (North-Holland, Amsterdam, 2003), Vol. 45 .
[44] A. Yamilov, S. H. Chang, A. Burin, A. Taflove, and H. Cao, Phys. Rev. B **71**, 092201 (2005).
[45] H. Yu, J. Park, K. Lee, J. Yoon, K. Kim, S. Lee, and Y. K. Park, Curr. Appl. Phys. **15**, 632 (2015).
[46] R. Sarma, T. Golubev, A. Yamilov, and H. Cao, Appl. Phys. Lett. **105**, 041104 (2014).

Supplementary Information: Shape-dependence of transmission, reflection and absorption eigenvalue densities in disordered waveguides with dissipation

A. Yamilov,[1,*] S. Petrenko,[1] R. Sarma,[2] and H. Cao[2,†]

[1] *Department of Physics, Missouri University of Science and Technology, Rolla, Missouri 65409, USA*
[2] *Department of Applied Physics, Yale University, New Haven, CT, 06520, USA*

We consider a two-dimensional (2D) waveguide formed by reflecting boundaries at $y(z) = \pm W(z)/2$. The width of the waveguide $W(z)$ is a smooth function of z - the axial coordinate, see Fig. 1. The waveguide is coupled to two leads (empty waveguides) at $z = 0$ and $z = L$. The leads have constant width, $W_L = W(0)$ and $W_R = W(L)$, thus supporting $N_L = W_L/(\lambda/2)$ and $N_R = W_R/(\lambda/2)$ guided modes respectively. The transport through the disordered region $0 \le z \le L$ is assumed to be diffusive, i.e., $\ell \ll L \ll \xi$, where ℓ and ξ are transport mean free path and the localization length respectively, and the dimensionless conduction $g_p \gg 1$, where subscript p stands for "passive".

Derivation of density of the transmission eigenvalues: Circuit theory

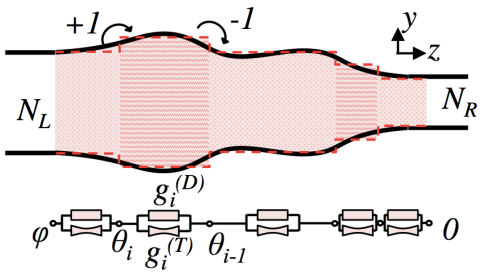

FIG. 1. Schematic representation of a disordered waveguide with varying width $W(z)$. It is approximated by a sequence of segments, each having a constant width W_i, with $W_i - W_{i-1} = \pm\lambda/2$ corresponding to adding/removing one waveguide mode with real propagation constant. Circuit theory [1] representation of the waveguide in terms of diffusive conductors (propagating modes) and tunneling junctions (evanescent modes) is depicted below.

In this section, we derive the bimodal distribution for the density of transmission eigenvalues in passive disordered waveguides of an arbitrary shape. Circuit theory was developed in Ref. [1] in context of mesoscopic transport of electrons in disordered conductors and tunneling junctions. However, the methodology is general and applicable to any system that exhibits phase coherent wave transport. Below we will apply it to light transport in a disordered waveguide to derive the density of transmission eigenvalues. The first step is to represent a complex system as a network of basic elements, in our case, diffusive conductors (resistors) and tunneling junctions, as follows.

As depicted in Fig. 1, a waveguide of variable width can be represented as a sequence of segments $z_{i-1} < z < z_i$ in which the number of waveguide modes (with real propagation constant) is $N_i = \text{floor}[W(z)/(\lambda/2)]$. The steps of $\Delta W = W_i - W_{i-1} = \lambda/2$ determine the length of each segment, and the number of waveguide modes in consecutive segments differs by ± 1. 1 (-1) corresponds to the conversion of an evanescent (propagating) mode with imaginary (real) valued propagation constant to the propagating (evanescent) one.

For a unified description of all segments, we assume each segment has $N_{max} = \max[W(z)]/(\lambda/2)$ modes. Hence the i'th segment has N_i propagating and $N_i^{(e)}$ evanescent modes so that $N_i + N_i^{(e)} = N_{max}$ for any i. To complete mapping onto a circuit network, see Fig. 1, we model wave transport via N_i propagating modes in the i'th segment as a diffusive conductor with dimensionless conductance $g_i^{(D)} \gg 1$ and $N_i^{(e)}$ evanescent modes as a tunneling junction with very small conductance $g_i^{(T)} \ll 1$. In fact, the evanescent modes [2] are not usually considered in theoretical models [3] because their contributions to the overall transport are negligible [4, 5]. Lastly we note that the diffusive conductor and tunneling junction are connected in parallel for each segment whereas the successive segments are connected in series.

Next we introduce the "phase" and the "matrix current" in such a network. The matrix current $\mathcal{I}$ is analogous to the current, and the phase ϕ to the electric potential in an electronic circuit, thus the phase drop across a circuit element determines the matrix current through it. Current-phase relationships are given by $\mathcal{I}_i^{(D)} = g_i^{(D)}(\theta_i - \theta_{i-1})$ and $\mathcal{I}_i^{(T)} = g_i^{(T)} \sin(\theta_i - \theta_{i-1})$ for the diffusive conductor and tunneling junction respectively [6]. $\mathcal{I}$ obeys Kirchhoff's rules which for our system in Fig. 1 gives $\mathcal{I}(\phi) = \mathcal{I}_i(\theta_i - \theta_{i-1}) = \mathcal{I}_i^{(D)}(\theta_i - \theta_{i-1}) + \mathcal{I}_i^{(T)}(\theta_i - \theta_{i-1})$. $\mathcal{I}_i^{(D)}$ and $\mathcal{I}_i^{(T)}$ represents matrix current through i'th diffusive conductor and tunneling junction respectively, and θ_i is the phase at node i. Applying these rules we find

$$\mathcal{I}(\phi) = g^{(CT)}\phi\,, \tag{1}$$

with

$$\frac{1}{g^{(CT)}} = \sum_{i=1}^{M} \frac{1}{g_i^{(D)} + g_i^{(T)}} \simeq \sum_{i=1}^{M} \frac{1}{g_i^{(D)}}\,, \tag{2}$$

where M is the number of segments, and the diffusive conductance of the i-th segment $g_i^{(D)} = (\pi/2)N_i\ell/(z_i - z_{i-1})$ is much larger than $g_i^{(T)}$.

The density of transmission eigenvalues follows from the relationship between $\mathcal{I}(\phi)$ and ϕ drop across the entire system [6]:

$$\mathcal{D}(\tau) = \frac{1}{2\pi\tau\sqrt{1-\tau}}\mathrm{Re}\left[\mathcal{I}\left(\pi - 0 + 2i\mathrm{arccosh}(\tau^{-1/2})\right)\right]. \quad (3)$$

Substituting Eqs. (1,2) into Eq. (3) we obtain the bimodal distribution with dimensionless conductance g_p given by Eq. (2). In the continuous limit, the summation over the segments in Eq. (2) is replaced with an integral as

$$g_p^{(CT)} = (k\ell/2)\left[\int_0^L W^{-1}(z)dz\right]^{-1}. \quad (4)$$

Scattering matrix of dissipative waveguides with varying cross-section

Scattering matrix $\hat{S}$ contains full information about the transport properties of a system. It is related to the transmission, reflection matrices for light incident from the left $\hat{t}$, $\hat{r}$ and right $\hat{t}'$, $\hat{r}'$ as follows:

$$\vec{a}^{\ out} = \begin{pmatrix} \vec{a}_L^{\ out} \\ \vec{a}_R^{\ out} \end{pmatrix} = \hat{S}\vec{a}^{\ in} = \begin{pmatrix} \hat{r} & \hat{t}' \\ \hat{t} & \hat{r}' \end{pmatrix}\begin{pmatrix} \vec{a}_L^{\ in} \\ \vec{a}_R^{\ in} \end{pmatrix}. \quad (5)$$

$\vec{a}_L^{\ in}$ and $\vec{a}_L^{\ out}$ are $N_L \times 1$ vectors for amplitudes of fields in the incoming/outgoing modes at $z < 0$, and $\vec{a}_R^{\ in}$ and $\vec{a}_R^{\ out}$ are $N_R \times 1$ vectors for amplitudes of the incoming/outgoing modes at $z > L$. The matrices are, in general, rectangular: $\hat{t}$ – $N_R \times N_L$, $\hat{r}$ – $N_L \times N_L$, $\hat{t}'$ – $N_L \times N_R$, $\hat{r}'$ – $N_R \times N_R$, and $\hat{S}$ – $(N_L + N_R) \times (N_L + N_R)$. In passive systems, due to conservation of flux ($\hat{S}^\dagger\hat{S} = \hat{I}$), time-reversal symmetry ($\hat{S}^*\hat{S} = \hat{I}$), and optical reciprocity ($\hat{S}^T = \hat{S}$), the non-zero eigenvalues are identical for $\hat{t}^\dagger\hat{t}$, $\hat{I} - \hat{r}^\dagger\hat{r}$, $\hat{t}'^\dagger\hat{t}'$, $\hat{I} - \hat{r}'^\dagger\hat{r}'$ matrices, i.e., $\tau = 1 - \rho = \tau' = 1 - \rho'$. The number of non-zero eigenvalues in a disordered waveguide is given by $\min(N_L, N_R)$.

A distinct group of evanescent eigenchannels arises in waveguides with a constriction $N_L, N_R > N_{min}$. This can be traced to the fact that the number of waveguide modes with real propagation constants is width dependent: $N(z) = W(z)/(\lambda/2)$. A constriction reduces the number of propagating modes and causes the rest to become evanescent. Although these modes can still transfer energy via tunneling and scattering in and out of the propagating modes, the inefficient transport [4, 5] results in exponential attenuation of their amplitudes $\sim \exp[-d/\lambda]$. The consequence of the attenuation can be better understood in terms of transfer matrix $\hat{M}_i$ of each segment of the waveguide, see Fig. 1. Unlike $\hat{S}$ matrix, the transfer matrix relates the incoming and outgoing waves on the left to those on the right (compare to Eq. 5)

$$\begin{pmatrix} \vec{a}_R^{\ out} \\ \vec{a}_R^{\ in} \end{pmatrix} = \hat{M}\begin{pmatrix} \vec{a}_L^{\ in} \\ \vec{a}_L^{\ out} \end{pmatrix}. \quad (6)$$

which makes it multiplicative $\hat{M} = \Pi_i \hat{M}_{i=1}^M$. It is now easy to see that a set of small eigenvalues in one segment leads to small eigenvalues in the overall matrix $\hat{M}$. This observation can be restated mathematically as following: the rank of a product cannot exceed the smallest rank of the multiplier matrices [7]. Because the transfer and transmission matrices are related [3, 8] via

$$\left[1 + \hat{M}\hat{M}^\dagger + \left(\hat{M}\hat{M}^\dagger\right)^{-1}\right]^{-1} = \frac{1}{4}\begin{pmatrix} \hat{t}\hat{t}^\dagger & 0 \\ 0 & \hat{t}'\hat{t}'^\dagger \end{pmatrix}, \quad (7)$$

every small eigenvalue of $\hat{M}\hat{M}^\dagger$ should have the counterpart of $\hat{t}\hat{t}^\dagger$ or $\hat{t}'\hat{t}'^\dagger$. Likewise, $2N_{min}$ finite eigenvalues of $\hat{M}\hat{M}^\dagger$ corresponds to N_{min} finite eigenvalues of $\hat{t}\hat{t}^\dagger$ and N_{min} of $\hat{t}'\hat{t}'^\dagger$. Therefore, if certain eigenvalues become small in some of $\hat{M}_i$ (e.g. in a constriction) they remain small in $\hat{M}$ and in both $\hat{t}\hat{t}^\dagger$ and $\hat{t}'\hat{t}'^\dagger$. These small eigenvalues correspond to the *evanescent eigenchannels*. They are distinct from closed eigenchannels with $\tau > \tau_C \sim \exp[-L/\ell] \gg \exp[-d/\lambda]$. The latter inequality follows from $\lambda \ll \ell$.

In systems with absorption, in contrast, optical reciprocity is the only constraint left. It leads to $\hat{t} = \hat{t}'^T$, $\hat{r} = \hat{r}^T$, $\hat{r}' = \hat{r}'^T$, where superscript T denotes matrix transpose. Despite the fact that non-zero eigenvalues of $\hat{t}^\dagger\hat{t}$ and $\hat{t}'^\dagger\hat{t}'$ are still identical, they are no longer related to those of the reflection matrices because input energy can be absorbed instead of being transmitted or reflected.

Numerical simulations

Numerical simulations are based on Kwant software package [9]. It allows one to conveniently compute $\hat{S}$ matrix of disordered waveguide defined as a collection of coupled lattice sites $|i\rangle$ in two dimensional grid described by a tight-binding Hamiltonian

$$\hat{H}|\psi\rangle = \left[\sum_{i,j} H_{ij}|i\rangle\langle j|\right]\left(\sum_l \psi_l|l\rangle\right), \quad (8)$$

where ψ_l is the wavefunction (i.e. field) amplitude at site l (a 2D vector), see Fig. 2. We introduce disorder by adding a random on-site potential δE_{ii} to the diagonal elements $H_{ii} = E_0 + \delta E_{ii}$, while keeping the nearest neighbor coupling at constant value of 1. The scattering region $0 \le z \le L$ is connected to the leads – infinitely long waveguides with $\delta E_{ii} = 0$.

The model is well suited to describe continuous wave scattering phenomena as long as $k\ell \gg 1$. In our simulation we choose the parameter E_0 and the disorder strength

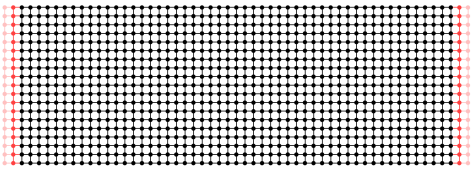

FIG. 2. Transport in a waveguide, which consists of a collection of coupled lattice sites, is described by the Hamiltonian in Eq. (8). The disordered region (black dots) is connected to two infinitely long leads (red dots) on the left and right.

Δ ($-\Delta < \delta E_{ii} < \Delta$) so that $k\ell \simeq 60$. Because $\langle \delta E_{ii} \rangle = 0$, the average value of H_{ii} does not change with the strength of disorder, avoiding any impedance mismatch between the leads and the random waveguide [10]. To eliminate the ballistic component that propagates through the system without scattering, we set $L/\ell \simeq 30 \gg 1$.

The transport mean free path ℓ is obtained from the value of dimensionless conductance g_p statistically averaged over an ensemble of disorder realizations. In passive rectangular waveguide $g_p = (\pi/2)N\ell/L$ uniquely determines ℓ.

To ensure diffusive transport ($g_p \gg 1$) in the simulated waveguides, we select the number of modes (i.e. the width of the waveguides) to be sufficiently large - on the order of hundreds.

Absorption is introduced to our system by adding a small constant negative imaginary part γ to the on-site potential $E_0 \to E_0 + i\gamma$. The specific value of γ is selected to obtain the desired value of the diffusive absorption length ξ_a. The latter is obtained from $g = (\pi N\ell/\xi_a)\exp[-L/\xi_a]$ for a rectangular waveguide with $L/\xi_a \gg 1$ [11]. The conductances in the four systems are $g = 12.1\ 12.3,\ 11.3,\ 12.3$, $g = 2.6\ 2.6,\ 1.9,\ 2.8$, and $g = 0.13\ 0.12,\ 0.08,\ 0.14$ in the weak, intermediate and strong regimes respectively. To obtain the densities of transmission, reflection and absorption eigenvalues in Figs. 1-4, we perform simulations for 1000 random realizations of δE_{ij}, giving us $\sim 2 \div 5 \times 10^5$ eigenvalues with a sufficiently low noise over six decades of magnitude.

Crossover from quasi-1D to 2D geometry

In passive random media, the universal bimodal distribution of transmission eigenvalues has been shown [12] to apply to arbitrary geometries and not just to the quasi-1D waveguides ($W/L \ll 1$) as originally assumed in Ref. [13]. In Fig. 3a, we confirm this result for passive constant-width waveguides with both $W/L < 1$ and $W/L > 1$. The density of transmission eigenvalues exhibits no dependence on W/L – the distribution function indeed remains universal.

When absorption is introduced to the waveguide, the eigenvalue distribution is modified, as predicted in [11]. As shown in Fig. 3(b-d), the density of transmission eigenvalues does not depend on the waveguide width W, instead it depends only on the ratio of waveguide L to the diffusive absorption length ξ_a. The distribution function remains identical for waveguides of width $W < \xi_a$ and $W > \xi_a$, as long as the ratio L/ξ_a is fixed. These results confirm that the universal distribution function for the transmission

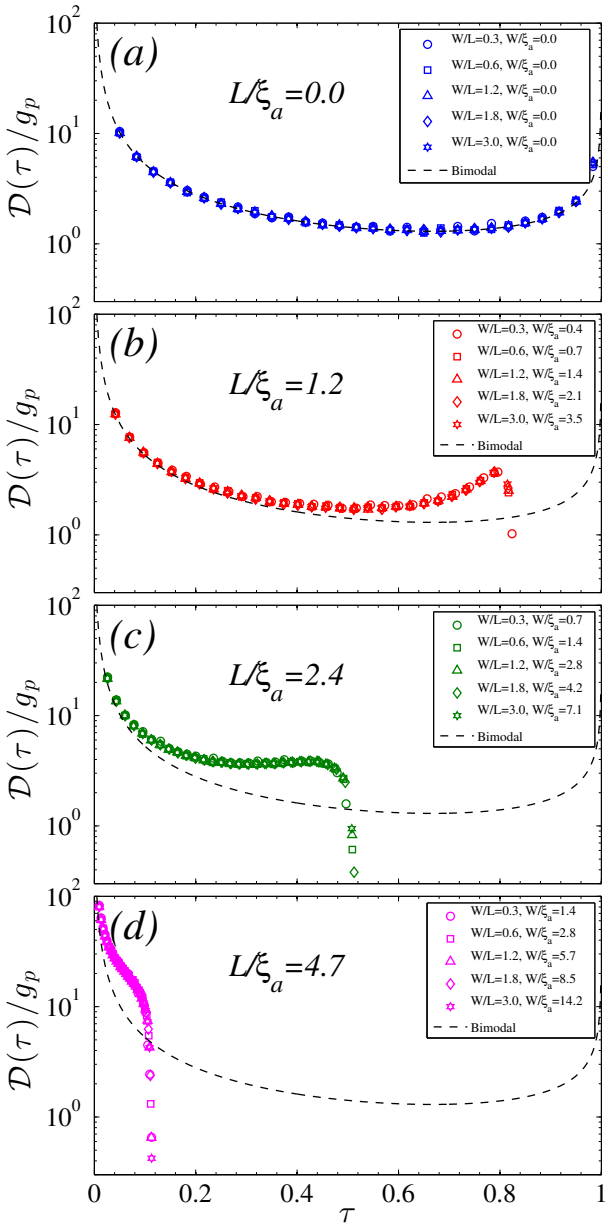

FIG. 3. The effect of parameters L/W, L/ξ_a, and W/ξ_a on the normalized density of transmission eigenvalues $\mathcal{D}(\tau)/g_p$ in rectangular waveguides without (a) and with absorption (b-d). Panels (a-d) correspond to $L/\xi_a = 0$, 1.2, 2.4 and 4.7 respectively. In each panel, densities obtained for different ratios of W/L (different data sets defined in the legend) coincide, showing that L/ξ_a is the only parameter that determines the functional form of the density of transmission eigenvalues. Dashed line in each panel is the bimodal distribution for the waveguides without absorption.

eigenvalues is not modified in the crossover regime, even in the presence of absorption.

Density of the absorption eigenvalues with two-sided excitation

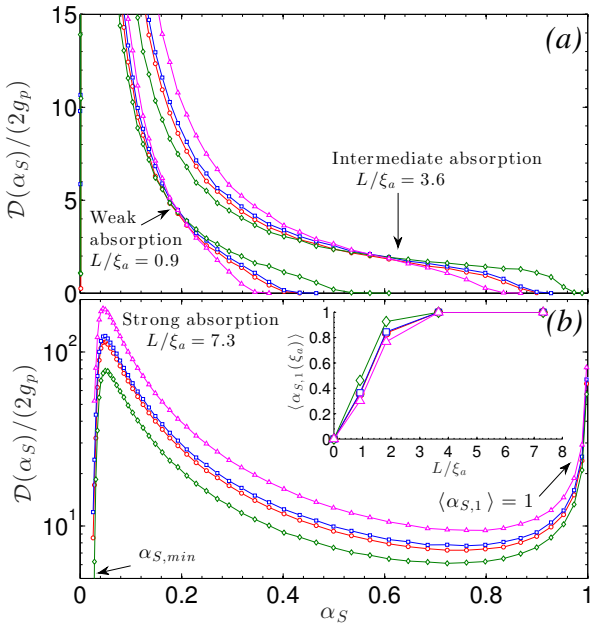

FIG. 4. Density of absorption eigenvalues α_S with two-sided illumination at weak absorption $\langle \alpha_{S,1} \rangle \ll 1$, intermediate absorption $\langle \alpha_{S,1} \rangle \lesssim 1$ (panel a), and strong absorption $\langle \alpha_{S,1} \rangle \simeq 1$ (panel b). Symbol notations for rectangular, horn, lantern, and bow-tie waveguides are the same as in Fig. 3 of the main text. With increasing absorption, $\mathcal{D}(\alpha_S)$ develops a long tail at large α_S, which eventually becomes a peak at $\alpha_S \simeq 1$. In all cases $\mathcal{D}(\alpha_S)$ shows strong dependence on the shape of the waveguide. The inset of panel (b) plots the ensemble-averaged largest eigenvalue $\langle \alpha_{S,1} \rangle$ vs. the absorption strength L/ξ_a.

Fig. 4 in the main text shows the density of α – eigenvalues of $\hat{A} \equiv \hat{I} - \hat{t}^\dagger \hat{t} - \hat{r}^\dagger \hat{r}$ for waves incident from the left lead or $\hat{A}' \equiv \hat{I} - \hat{t}'^\dagger \hat{t}' - \hat{r}'^\dagger \hat{r}'$ for the wave incident from the right lead. In contrast, the eigenvalues α_S of the matrix $\hat{A}_S \equiv \hat{I} - \hat{S}^\dagger \hat{S}$ correspond to eigenvectors with waves incident from both leads simultaneously – *two-sided excitation*, see Eq. (5).

Figure 4 shows evolution of the density of eigenvalues α_S, $\mathcal{D}(\alpha_S)$, with absorption. While it is qualitatively similar to $\mathcal{D}(\alpha)$ in Fig. 4 of the main text, we notice the following differences. First, unlike one-sided excitation case where $\mathcal{D}(\alpha)$ can be dependent of the input direction in an asymmetric waveguide (e.g. $\mathcal{D}_L(\alpha) \neq \mathcal{D}_R(\alpha)$ in a horn waveguide), there is only one $\mathcal{D}(\alpha_S)$. The number of $\alpha_{S,n}$ in any given sample is $N_L + N_R$, greater than that of α_n $(= N_L)$ or of α'_n $(= N_R)$. Secondly, in the regimes of weak and intermediate absorption, the density of $\mathcal{D}(\alpha_S)$ exhibits long tails toward $\alpha_S \to 1$, c.f. Fig. 4a, whereas $\mathcal{D}(\alpha)$ has already developed a second peak, c.f. Fig. 4a of the main text. Third, because of the tail of $\mathcal{D}(\alpha_S)$, eigenvalues close to unity ($\alpha_S \simeq 1$) can be found at the amount of absorption smaller than that for $\mathcal{D}(\alpha)$, which exhibits a sharp dropoff beyond the second peak. The latter conclusion can be understood intuitively: two-sided excitation allows for a greater degree of input control. In strong absorption regime, our results coincide with the results of Ref. [14], where the concept of coherent enhancement of absorption was first proposed.

Existing theoretical description of $\mathcal{D}(\tau)$ in rectangular waveguides with absorption

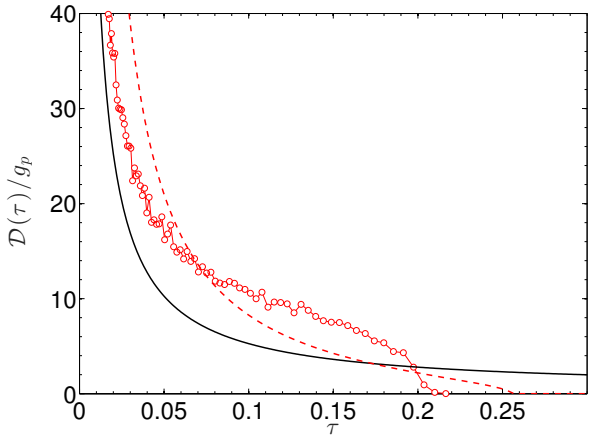

FIG. 5. Normalized density of the transmission eigenvalues $\mathcal{D}(\tau)/g_p$ in rectangular waveguide with absorption $L/\xi_a = 3.6$ (circles). Solid line is the bimodal distribution shown for reference. Dashed line plots Eqs. (10,12) (not a fit) for $L/\xi_a = 3.6$ sample.

Fig. 2 of the main text we present the results of numerical simulations of $\mathcal{D}(\tau)$ in absorbing disordered waveguides. In this section we briefly review the previous theoretical model in Ref. [11], and apply it to describe the density of transmission eigenvalues in *rectangular waveguides*.

We begin by introducing a resolvent

$$G(z) = \left\langle \mathrm{Tr} \frac{1}{z - \hat{t}^\dagger \hat{t}} \right\rangle, \tag{9}$$

which formally defines the eigenvalue density as

$$\mathcal{D}(\tau) = -(1/\pi)\mathrm{Im}[G(\tau + i0)]. \tag{10}$$

In passive systems, $G(z)$ has been found in several works (see Ref. [6] for review):

$$G_0(z) = \frac{N}{z} - \frac{g_p}{z\sqrt{1-z}} \mathrm{arctanh}\left[\frac{\tanh(N/g_p)}{\sqrt{1-z}}\right], \tag{11}$$

which leads to the bimodal distribution in the main text.

In Ref. [11], Brouwer obtained an approximate analytical expression for $G(z)$, and hence for $\mathcal{D}(\tau)$ in the limit of strong absorption $L/\xi_a \gg 1$. The result reads

$$G^{(B)}(z) = \frac{N}{z} - \frac{2g_p}{z}\,\mathcal{W}\left(-\frac{L}{\xi_a z}e^{-L/\xi_a}\right), \qquad (12)$$

where $\mathcal{W}(z)$ is Lambert W-function. This expression is plotted in Fig. 5 with a dashed line for $L/\xi_a = 3.6$. It is not a fit, because all parameters in Eq. (12) are known independently. We observe that Eqs. (10,12) overestimates the maximum value of τ and underestimates the density at small τ ($\lesssim 0.2$). We attribute these deviations to insufficiently large value of the absorption parameter L/ξ_a, which does not reach the strong absorption limit required for deriving Eq. (12). Lastly, it is not immediately clear how this model can be generalized to the waveguides with varying width.

* yamilov@mst.edu
† hui.cao@yale.edu

[1] Y. V. Nazarov, Superlatt. and Microstruct. **25** (1999).
[2] P. F. Bagwell, Phys. Rev. B **41**, 10354 (1990).
[3] C. W. Beenakker, Rev. Mod. Phys. **69**, 731 (1997).
[4] L. S. Froufe-Pérez, M. Yépez, P. A. Mello, and J. J. Sáenz, Phys. Rev. E **75**, 031113 (2007).
[5] B. Payne, T. Mahler, and A. Yamilov, Waves in Random and Complex Media **23**, 43 (2013).
[6] Y. V. Nazarov and Y. M. Blanter, *Quantum Transport: Introduction to Nanoscience* (Cambridge Univ. Press, 2009).
[7] J. R. Magnus and H. Neudecker, *Matrix differential calculus with applications in statistics and econometrics* (John Wiley, New York, 1999).
[8] J. L. Pichard, N. Zanon, Y. Imry, and A. D. Stone, J. Phys. France **51**, 587 (1990).
[9] C. W. Groth, M. Wimmer, A. R. Akhmerov, and X. Waintal, New J. Phys. **16**, 063065 (2014).
[10] X. Cheng, C. Tian, and A. Z. Genack, Phys. Rev. B **88**, 094202 (2013), 10.1103/PhysRevB.88.094202.
[11] P. W. Brouwer, Phys. Rev. B **57**, 10526 (1998).
[12] Y. V. Nazarov, Phys. Rev. Lett. **73**, 134 (1994).
[13] O. N. Dorokhov, Solid State Comm. **51**, 381 (1984).
[14] Y. D. Chong and A. D. Stone, Phys. Rev. Lett. **107**, 163901 (2011).